Differential network analysis reveals the key role of the ECM-receptor pathway in α-particle-induced malignant transformation

Wenying Yan,[1,2,7] Wentao Hu,[3,7] Yidan Song,[1,7] Xingyi Liu,[1] Ziyun Zhou,[1,2] Wanshi Li,[3] Zhifei Cao,[4] Weiwei Pei,[3] Guangming Zhou,[3] and Guang Hu[1,2,5,6]

[1]MOE Key Laboratory of Geriatric Diseases and Immunology, Suzhou Key Laboratory of Pathogen Bioscience and Anti-infective Medicine, Department of Bioinformatics, Center for Systems Biology, School of Biology and Basic Medical Sciences, Suzhou Medical College of Soochow University, Suzhou 215213, China; [2]Jiangsu Province Engineering Research Center of Precision Diagnostics and Therapeutics Development, Soochow University, Suzhou 215123, China; [3]State Key Laboratory of Radiation Medicine and Protection, School of Radiation Medicine and Protection, Collaborative Innovation Center of Radiological Medicine of Jiangsu Higher Education Institutions, Soochow University, Suzhou 215123, China; [4]Department of Pathology, the Second Affiliated Hospital of Soochow University, Suzhou 215004, China; [5]Key Laboratory of Alkene-carbon Fibres-based Technology & Application for Detection of Major Infectious Diseases, Soochow University, Suzhou 215123, China; [6]Jiangsu Key Laboratory of Infection and Immunity, Soochow University, Suzhou 215123, China

Space particle radiation is a major environmental factor in spaceflight, and it is known to cause body damage and even trigger cancer, but with unknown molecular etiologies. To examine these causes, we developed a systems biology approach by focusing on the co-expression network analysis of transcriptomics profiles obtained from single high-dose (SE) and multiple low-dose (ME) α-particle radiation exposures of BEAS-2B human bronchial epithelial cells. First, the differential network and pathway analysis based on the global network and the core modules showed that genes in the ME group had higher enrichment for the extracellular matrix (ECM)-receptor interaction pathway. Then, collagen gene COL1A1 was screened as an important gene in the ME group assessed by network parameters and an expression study of lung adenocarcinoma samples. COL1A1 was found to promote the emergence of the neoplastic characteristics of BEAS-2B cells by both *in vitro* experimental analyses and *in vivo* immunohistochemical staining. These findings suggested that the degree of malignant transformation of cells in the ME group was greater than that of the SE, which may be caused by the dysregulation of the ECM-receptor pathway.

INTRODUCTION

Spaceflight imposes a unique suite of environmental effects on biology.[1] With the expansion of spaceflight, the space environment includes unique hazards such as radiation exposure, which can adversely affect biological systems.[2,3] The main effect of radiation exposure is damage to DNA, including base damage, single-strand breaks, double-strand breaks, chromosomal aberrations, micronuclei, and genomic instability.[4–7] At the phenotypic level, radiation exposure leads to physical damage, including muscle and bone loss, neurological damage, and impaired immunity.[8] Space radiation exposure can also result in defects in mitochondrial physiology,

leading to numerous pathological conditions, including bone loss[9] and accelerated aging.[10] The primary concern for radiation exposure is the risk of developing tumors and/or cancer,[11] and the known increased cancer risk is caused by chronic low doses of radiation exposure.[12,13] However, the mechanism underlying the carcinogenic potential of radiation exposure is not fully understood, especially after chronic low doses of radiation exposure, which is the situation that astronauts must confront in long-term deep space missions.[14]

Knowledge of spaceflight injury has grown immensely in recent years, benefiting from large-scale "omics" technologies,[15] making an understanding of molecular mechanisms at the systems level possible. In 2020, Gertz et al.[16] integrated transcriptomic and proteomic data to study how spaceflight affects innate immunity through mitochondrial processes. This study, together with data from NASA's GeneLab (https://genelab.nasa.gov/),[17] opened the door to the study of

spaceflight in the big data era.[18–21] Multiomics cancer models integrating genomics, genome conformation, transcriptomics, and epigenomics have been used to predict how mutations from spaceflight radiation and cytoskeletal remodeling/DNA modification aberrations due to microgravity affect astronauts.[22] Due to the complexity of spaceflight biology, including different environmental factors such as particle radiation exposure and microgravity, systems biology approaches leveraging network modeling are required to characterize these components in a holistic fashion.[8]

Gene function is not isolated but forms protein-protein interaction networks (PPINs) governed by universal laws, and the network effect of genes is the driving force moving from the normal to the exposure group in response to environmental changes.[23] Thus, elucidating the changes in individual nodes and edges, distinct modules, and the entire network as a whole in terms of several network centrality parameters may provide functional information to describe such biological processes.[24] Differential network analysis can capture changes between conditions in the interplay between molecules, rather than changes in single molecules, and has many applications, including illuminating the molecular basis of tissue-selective processes or disease-specific genes,[25] and identifying critical signaling pathways altered during tumor transformation and progression,[26,27] or between different cancer subtypes.[28] On the other hand, biological networks, including PPINs, are intrinsically modular, with proteins belonging to the same module usually sharing common functions.[29,30] The identification of network clusters not only helps us to reveal the modular organization of cell signaling networks,[31] but also identifies functional modules in different conditions and in radiation biology.

In this work, employing transcriptome data associated with two different α-particle radiation methods (single high-dose irradiation [SE] and multiple low-dose irradiations [ME]) on human lung epithelial cells, we applied an unbiased multiple-level differential network analysis framework for systematically investigating the network changes that mimic the spaceflight environment (Figure 1). First, two weighted PPINs were constructed for two different α-particle radiation groups. Second, the difference between these networks was investigated through module differential analysis to identify the functional modules. Third, the functional enrichment and topological analyses were performed for the functional module, aiming to reveal key pathways and genes. Finally, the biological functionality of the identified hub genes was validated through experimental verification.

RESULTS

Data comparison of exposure groups with the control group and The Cancer Genome Atlas lung samples

The expression profiles of nine SE samples, nine ME samples, and three controls were obtained from RNA-sequencing (RNA-seq) (Figure 2A). Initially, we performed principal-component analyses (PCAs) on the expression profiles, and the results showed differences between the control groups and exposure groups (Figure 2B). All the control groups clustered close together, while the SE and ME samples clustered into two groups, indicating a relatively high degree of similarity of the exposure groups, and this expression pattern changed after exposure, regardless of the exposure methods.

The risk model of lung cancer from α-particle radiation has been primarily established based on BEAS-2B cells.[32] To evaluate the different exposure methods on BEAS-2B cells, we also performed correlation analysis between SE groups with normal lung samples and ME groups with normal lung samples. As shown in Figure 2C, both groups were significantly correlated with normal lung samples, but the correlation coefficients for the former comparison were significantly larger than those for the latter comparison, indicating that the SE groups were more similar to the control than the ME group; in other words, the cells under multiple exposures departed more from normality. Moreover, correlation analysis between R1_05_50 and lung cancer stage I samples, as well as between R25_05_50 and lung cancer stage I samples was performed (Figure 2D). The 50th passage samples were significantly correlated with the stage I samples, but the correlation coefficients for the former comparison were significantly smaller than that for the latter comparison, indicating that the ME groups were more similar to the stage I samples than the SE group.

Multiple exposures reveal genetic information and tumorigenesis-related pathways

Network theory provides new insights to study the disturbances of systems from global and local interactions. Here, we employed WGCNA and STRING to construct exposure way-specific PPINs (SENet and MENet) to compare the effects of single and multiple exposures on the cells (Figure 3A). As a result, SENet and MENet share the same network structure and topology (15,541 nodes and 4,385,019 links) but with different link weights. Then, we measured the consistency of the two networks by link weight distributions and RMSIP. As shown in Figure 3B, the weight distribution patterns of links in SENet and MENet were almost the same. However, the percentage of links with weights larger than 0.8 in SENet was larger than in MENet. In the RMSIP plot (Figure 3C), the RMSIP achieved 0.55, which means that SENet and MENet have a relatively high topological overlap rate. All the results indicated that SE groups were very similar to ME groups at the whole network level, but they still have their own respective characteristics.

We next calculated the topological centralities for genes in SENet and MENet to compare exposure effects from network features. As shown in Figures 3D and 3E, although the percentage of links with high weights in MENet was smaller than that in SENet, genes in MENet had significantly higher K and EC than those in SENet, which means that genes in MENet had more interactions and their neighbors also had more interactions. The results indicated that larger network wiring occurred with more perturbed genes and interactions induced by multiple exposures. Then, we investigated the function of hub genes with the top 5% degree in two networks using enrichment analysis of Kyoto Encyclopedia of Genes and Genomes (KEGG) pathways. There were 171 and 167 pathways that were significantly enriched
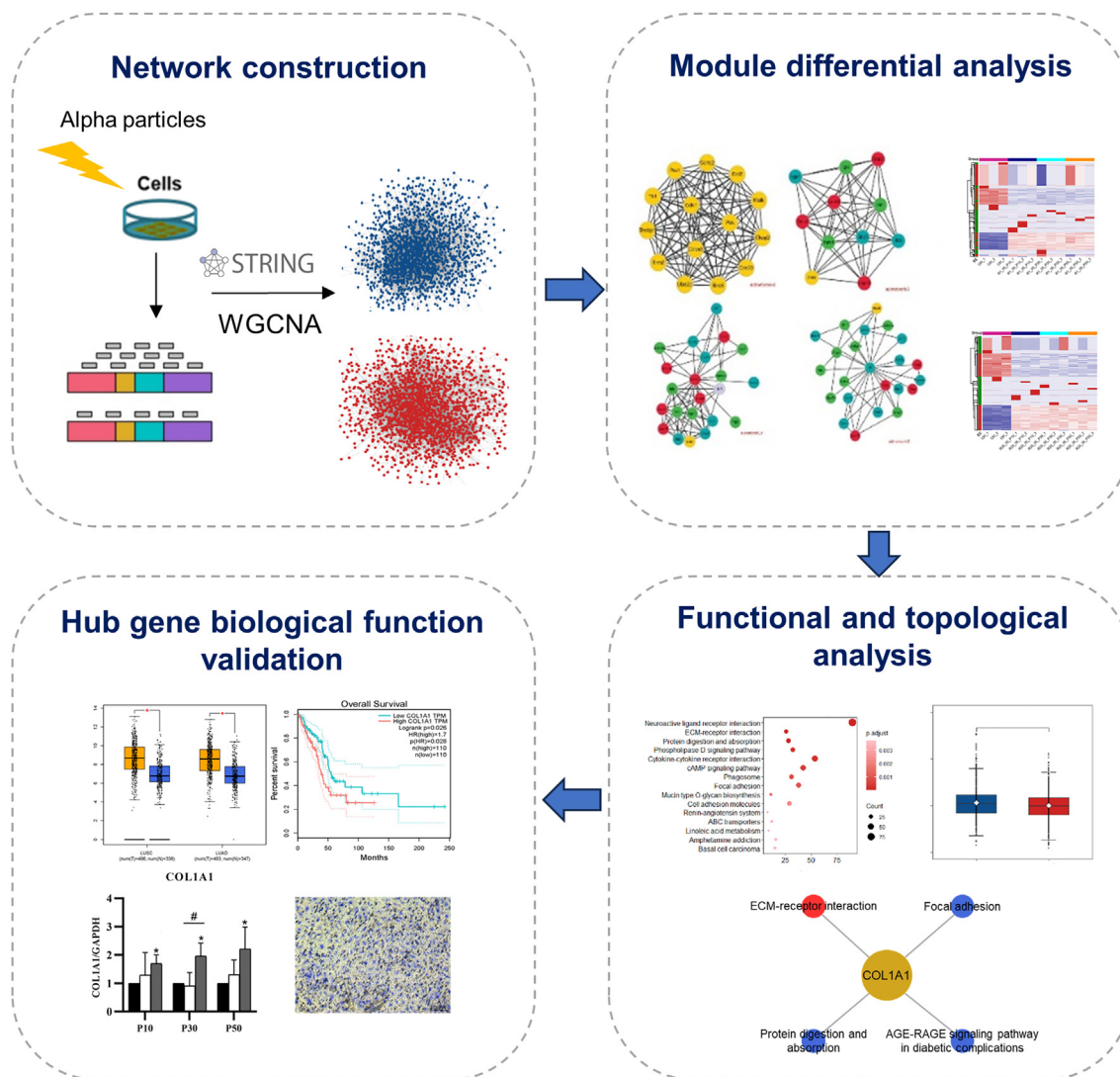
Figure 1. The differential network analysis framework

by the hub genes in SENet and MENet, respectively, and 153 of them were common pathways (Figure 3F), that is, enriched by the genes from both networks, which indicated that most hub genes in both networks have similar functions. However, they also have different pathways (Figure 3G). For hub genes in SENet, 18 pathways were significantly enriched, and two of them, the Fanconi anemia pathway and Homologous recombination, were related to DNA damage repair. When compared with SENet, MENet hub genes were specifically enriched in 14 pathways, which involved more genetic information processing-related pathways including Proteasome, Protein processing in the endoplasmic reticulum, DNA replication, as well as pathways associated with tumorigenesis, such as ECM-receptor interaction[33] and Ferroptosis.[34] All the results indicated that multiple exposures can cause more information exchange and that these interactions were related to tumorigenesis.

Comparison of single and multiple exposure effects on BEAS-2B cells from the network core

Important information always flows in the key interactions, which are always involved in the network core.[35] Therefore, we constructed the core network of SENet and MENet and compared their differences to characterize the single and multiple exposure effects on cells. First, we selected the interactions with weights larger than 0.40 and 0.45 in SENet and MENet as their core network, named SENetCore and MENetCore, respectively, to reflect the main important information flows among genes that were affected by different exposure conditions. SENetCore consists of 2,123 nodes and 9,847 interactions, while MENetCore consists of 2,129 nodes and 9,395 interactions. Then, the topological parameters were calculated for both network cores (Figure 4A; Figure S1). Similar to the whole network, the eigenvector centrality
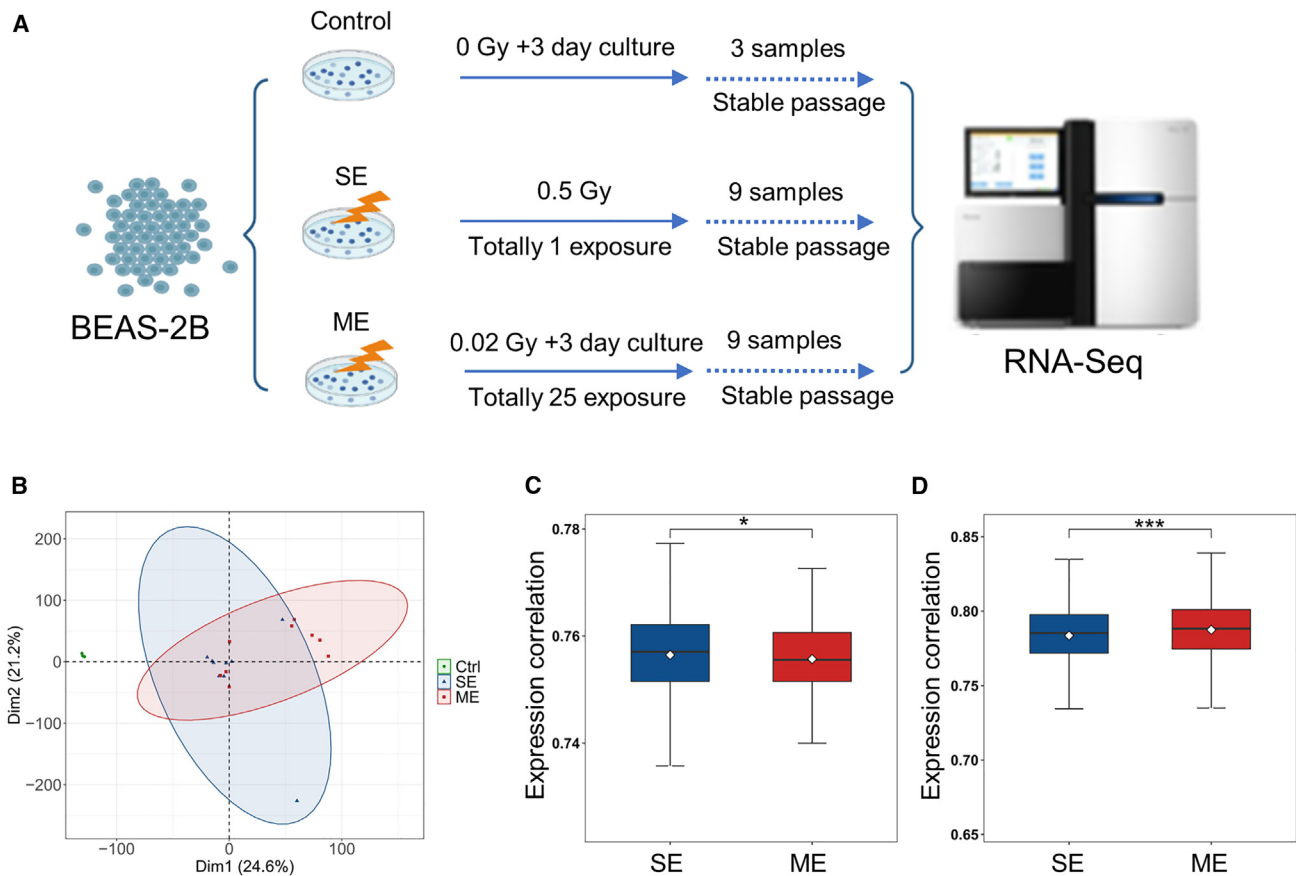
Figure 2. Experimental design and sample information

(A) RNA-seq of BEAS-2B cells after two types of irradiation. Three replicate controls were BEAS-2B cells without any treatment. SE: BEAS-2B cells after a single dose of 0.5 Gy and then sub-cultured to the 10th passage, 30th passage, or 50th passage. ME: BEAS-2B cells after 25 exposures of 0.02 Gy and then sub-cultured to the 10th passage, 30th passage, and 50th passage. (B) PCA plot depicting gene expression profiles for the control, SE, and ME groups. (C) Expression correlation of SE groups with normal lung samples, and ME groups with normal lung samples. (D) Expression correlation of R1_05_50 samples with lung cancer stage I samples and R25_05_50 samples with lung cancer stage I samples. $*p < 0.05$, $**p < 0.01$, $***p < 0.001$.

(EC) values of nodes in MENetCore were significantly larger than those in SENetCore, and they distinguished the control groups from both SE and ME groups (Figure 4B). The results indicated that in MENetCore, not only hub genes are important, but their neighbors also play important roles in the network, which indicates that multiple exposures may induce interactions among genes with a high information flow context.

To explore the functional differences between SENetCore and MENetCore, pathway enrichment analysis was performed, and the results demonstrated that both were enriched in the neuroactive ligand-receptor interaction, cytokine-cytokine receptor interaction, cAMP signaling pathway, and others (Figure 4C), indicating that both network cores also have similar biological functions. However, more importantly, some specific biological pathways were highlighted. In particular, the ECM-receptor interaction was significantly enriched in the ME groups at the network core level, again playing an important role in the ME group. Consistent with the whole

network findings, all the network core results indicate that MENetCore genes were more closely associated with tumors than SENetCore genes.

Network analysis reveals the conservation of the ECM-receptor pathway and hub genes in the ME group

We next performed module analysis for SENetCore and MENetCore to organize the exposure type-related changes in an unbiased manner. The Girvan-Newman and label propagation analysis algorithms were used together to find the robust modules in both networks. With a similar number of genes, SENetCore and MENetCore were divided into 98 and 76 modules, respectively. As shown in Figure 5A, there were more modules whose sizes were less than 100 in SENetCore than in MENetCore, and both networks had three modules with more than 100 genes. The results indicated that modules in MENetCore are more robust, which may suggest the biological importance of its functional modules.
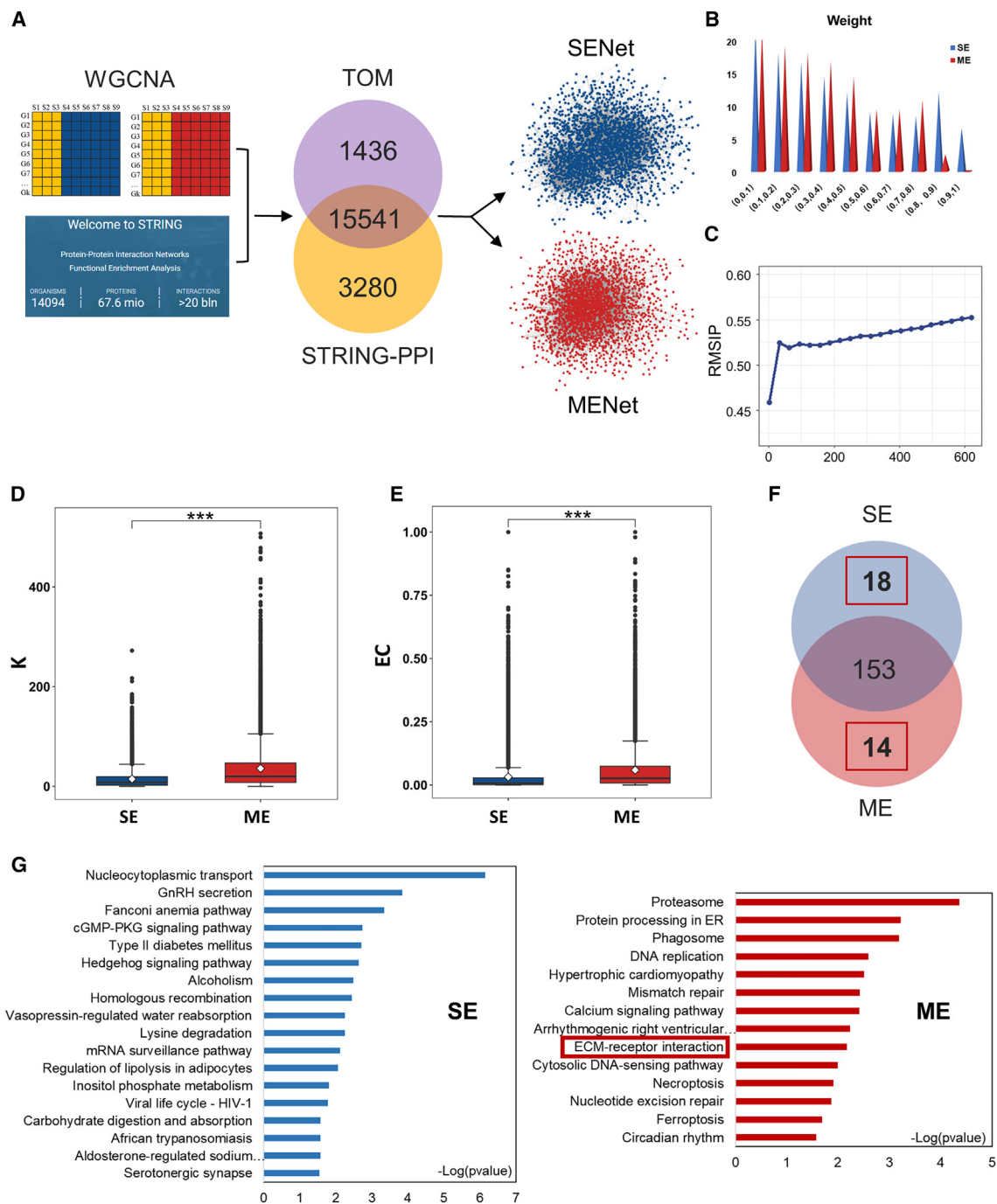
Figure 3. SENet and MENet

(A) Construction of exposure way-specific SENet and MENet PPINs. (B) Edge weight distribution in SENet and MENet. (C) Consistency between SENet and MENet. (D) Degree and (E) eigenvector centrality were significantly larger in MENet than in SENet. (F) Venn diagram showing overlap of significantly enriched pathways for the top 5% high degree in SENet (blue) and MENet (pink). (G) The significantly enriched pathways specific to the SE group (blue) and ME group (red). *$p < 0.05$, **$p < 0.01$, ***$p < 0.001$.

We also applied pathway enrichment analysis to analyze the functional enrichment of the three largest modules in SENetCore and MENetCore (Figure 5B). The results revealed that the largest mod-

ule in both network cores significantly enriched several of the same pathways, such as axon guidance, basal cell carcinoma and Wnt signaling pathways. Nevertheless, as previously mentioned,
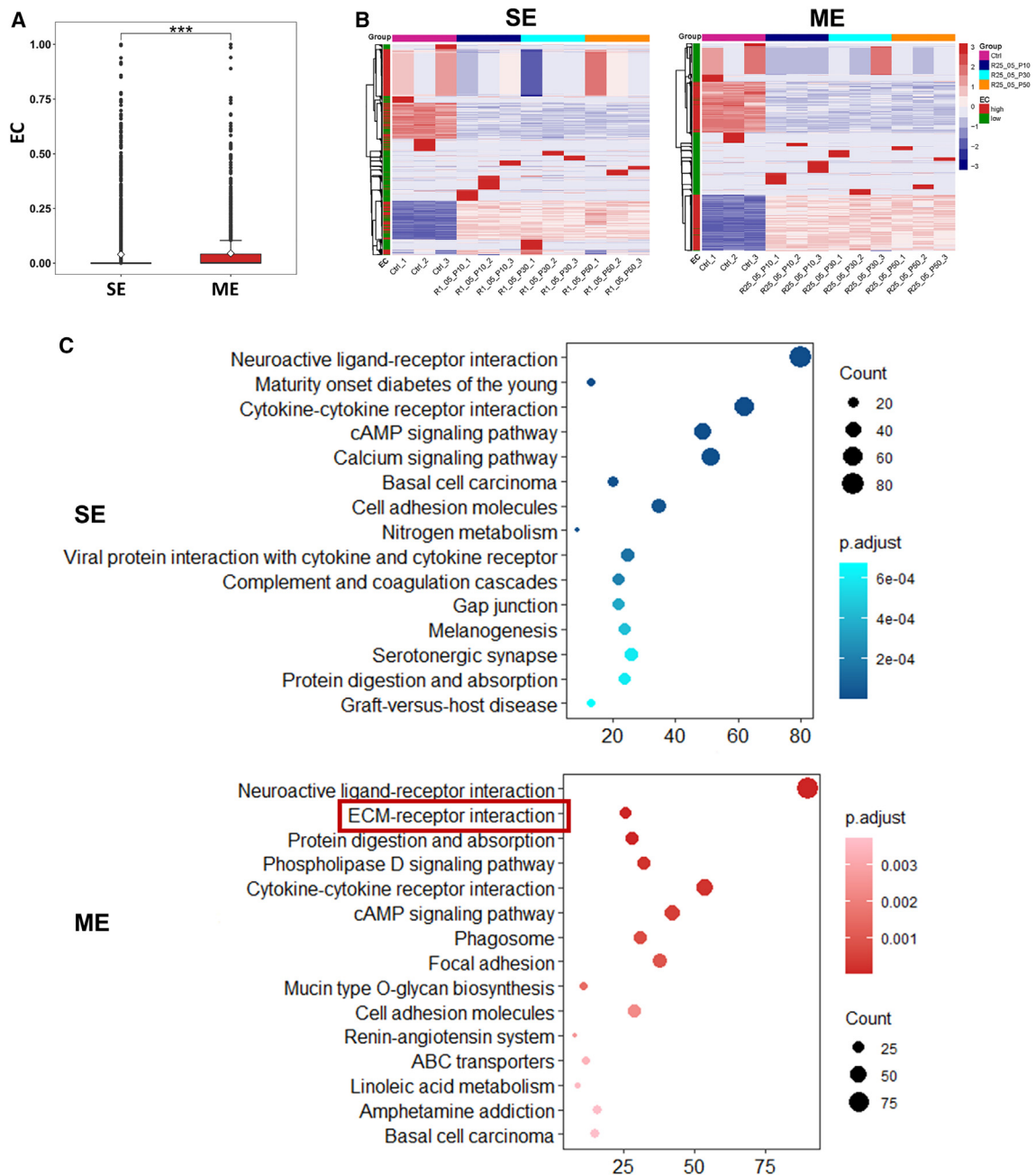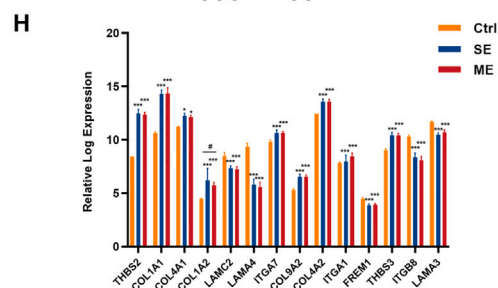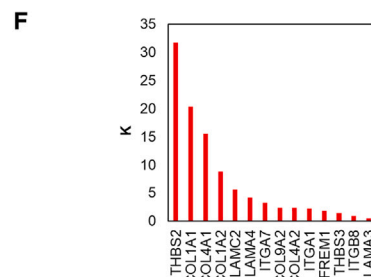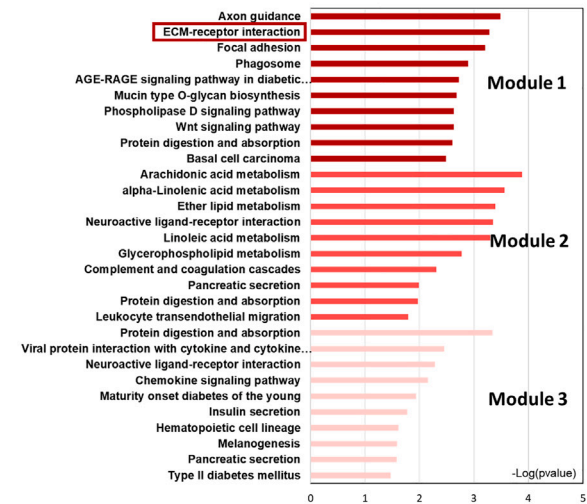
Figure 4. Network cores for SENet and MENet

(A) Boxplot representation of eigenvector centrality for SENetCore and MENetCore. (B) Heatmap representing the expression of genes in SENetCore and MENetCore. The color bar on the left represents the high and low (cutoff: median) EC values of genes that are matched, the right colored bar represents the expression level, and the upper colored bar represents the group. (C) Significantly enriched pathways for genes in SENetCore and MENetCore. *$p < 0.05$, **$p < 0.01$, ***$p < 0.001$.

the ECM-receptor interaction was again enriched by the largest module from the ME group, which indicated that multiple exposures might indeed affect the ECM-receptor interaction pathways.

To further explore the effect of exposure types on the modules, we mapped the differentially expressed genes (DEGs) between the SE group and control group, as well as the ME group and the control group, on the corresponding large modules (Figure 5C). In the SE
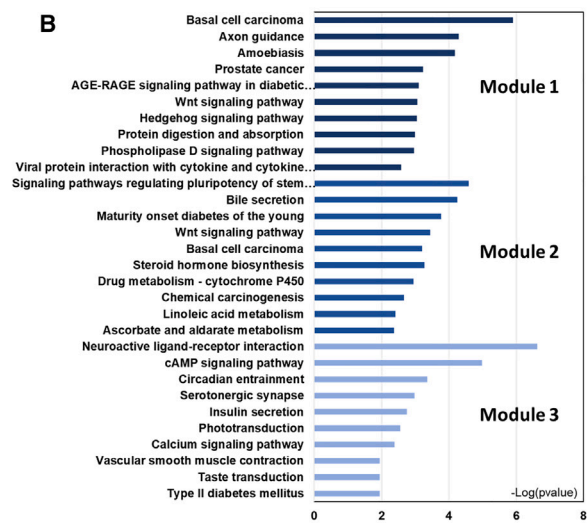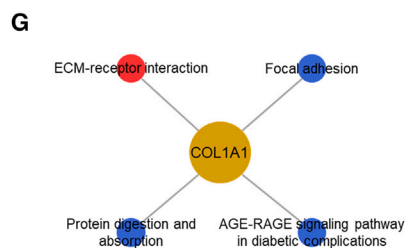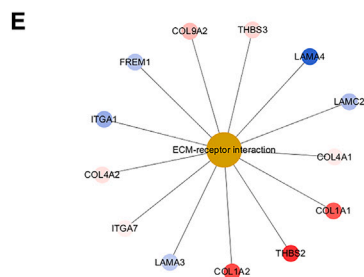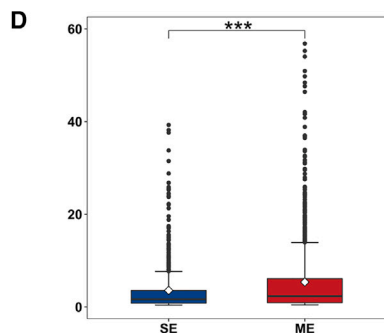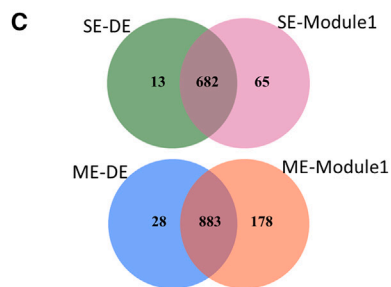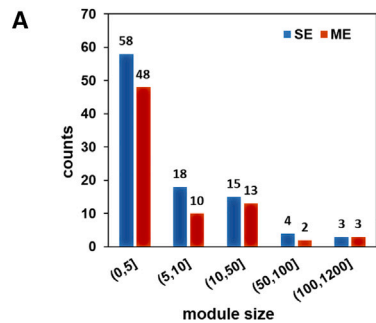
group, 682 DEGs were found in the largest module, but no DEGs and only one DEG was found in the second and third largest modules. Similarly, in the ME group, 883 DEGs were mapped in the largest module and no DEGs were mapped in the second and third largest modules. The results indicated that the largest module was the key module in the exposure-affected network, which captured most of the genes associated with expression changes. Moreover, we also calculated the intra-module topological parameters for the largest modules, and the results showed that the module in MENetCore had a significantly higher average degree than the module in SENetCore (Figure 5D). Other parameters for the largest three modules are listed in Table S1.

Owing to the conservation of ECM-receptor pathways at different network levels, we then focused on 14 genes in the largest module of MENetCore that are involved in this pathway (Figure 5E). Among them, five genes, THBS2, COL1A1, COL4A1, COL1A2, and LAMC2, were hub genes in the module (Figure 5F; Table S2). Although THBS2 has the largest centrality measures in the network level, COL1A1 is involved in more ECM-related pathways (Figure 5G), serving as a pathway crosstalk. In addition, most of the ECM-receptor pathway-mapped genes were up-regulated in the exposure groups compared with the controls (Figure 5H), among which COL1A1 was significantly up-regulated. Of note, the high degree in network and pathway levels (Figure S2), as well as the high expression of COL1A1 may suggest its important biological role, which needs further experimental investigation.

COL1A1 promotes the emergence of neoplastic characteristics in BEAS-2B cells

To further confirm which genes were driving the malignant transformation process, we examined each key gene in the ECM-receptor pathway and found that the mRNA level of COL1A1 was most significantly increased after single and multiple exposures (Figure S3). Then, the exposure effects of COL1A1 were further validated by bioinformatics through big data analysis, as well as through experimental expression data at both the RNA and protein levels. First, the expression level of COL1A1 was significantly higher in lung adenocarcinoma and lung squamous cell carcinoma cancer subtypes than in normal tissues, and its high expression was associated with poor survival outcomes (Figures S4A–S4C). Moreover, its expression level was also significantly increased in TNM stage samples, T_{1-4} samples, N_{0-3} samples, and M_{0-1} samples, when compared with normal samples (Figures S4D–S4G). Then, we measured COL1A1 expression levels in BEAS-2B cells and in the lung cancer cell lines Calu-1, and also in BEAS-2B cells after single and multiple exposures using qRT-PCR. As shown in Figures S5 and 6A, the expression of COL1A1 was significantly lower in BEAS-2B cells than in Calu-1 cells and

was significantly increased in BEAS-2B cells after single and multiple exposures. The results indicated that both single and multiple exposures can induce tumor-like high expression of COL1A1. In particular, COL1A1 was also up-regulated in the multiple exposure group R25_05_50 compared with the single exposure group R1_05_50, which indicated that the effects of multiple exposure were greater than those of single exposure on COL1A1 expression.

At the protein level, we evaluated the COL1A1 expression in SE and ME groups by western blot and found that the COL1A1 level was also significantly higher in the exposure compared with the control group (Figures 6B and 6C). In addition, COL1A1 protein was mainly localized to the cytoplasm of BEAS-2B cell lines (Figure 6D). Next, we conducted immunohistochemical analysis using a tissue microarray comprising 32 pairs of lung cancer and adjacent normal tissues and found that the ratio of COL1A1-positive cells in lung cancer tissue was significantly larger than in adjacent normal tissue (Figures 6E and 6F; Figure S6).

Finally, to examine the biological role of COL1A1 in the process of irradiation-induced cell transformation, we knocked down the expression of COL1A1 in normal, single, and multiple irradiated BEAS-2B cells by small interfering RNA (siRNA), respectively. The cells with COL1A1 knockdown were established *via* transfection and screening (Figure S6). We employed a loss-of-function approach using siRNA specifically targeting COL1A1. Following transfection of COL1A1-specific siRNA into the cells, the efficacy of gene silencing was assessed at both mRNA and protein levels (Figure S7). From the results, cells irradiated with single and multiple exposures of α-particles showed higher migration and invasion capacity, and in the COL1A1 knockdown cells, each group with COL1A1 knockdown exhibited significant decreases in migration and invasion abilities compared with the corresponding control group, especially in the irradiated group (Figures 6G and 6H; Figure S8). To elucidate the functional significance of COL1A1 in cellular transformation, we established a stable knockdown cell line using lentiviral-mediated short hairpin RNA (shRNA) specifically targeting COL1A1. The effectiveness of this knockdown strategy was rigorously assessed at both transcriptional and translational levels (Figure S9), and we also find that in the COL1A1 knockdown cell line, the number of soft agar colony formation was significantly reduced (Figures 6I and 6J).

The above results confirmed that irradiation could increase the expression level of COL1A1 at both RNA and protein levels regardless of the irradiation type, and the COL1A1 level was higher in the multiple exposure group. Therefore, we proposed that COL1A1 may be the key factor for irradiation-induced tumorigenesis, especially under multiple exposure conditions.

Figure 5. Network modules in SENetCore and MENetCore

(A) Module size distribution in the SE and ME groups. (B) The top 10 significantly enriched pathways of genes in the three largest modules in SENetCore (blue) and MENetCore (red). (C) Venn diagram showing the overlap of genes in the largest module with dysregulated genes in the SE and ME groups. (D) Boxplot representation of the degree in the largest module in SENetCore (blue) and MENetCore (red). (E) Module genes involved in ECM-receptor pathways. (F) Degree of ECM-receptor pathway-related genes in the module. (G) Four pathways in ME-Module 1 that COL1A1 are involved. (H) Expression of ECM-receptor pathway-related genes. *$p < 0.05$, **$p < 0.01$, ***$p < 0.001$.
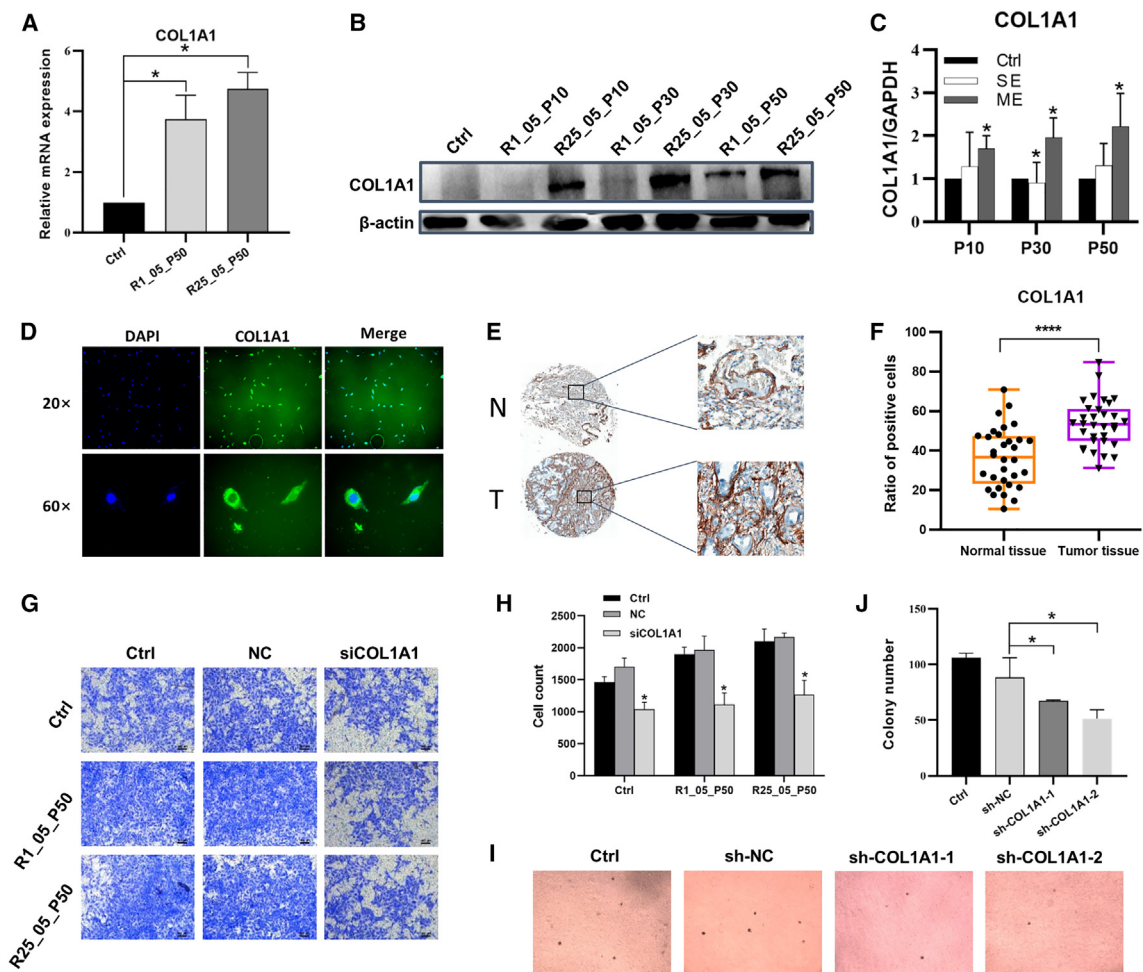
Figure 6. COL1A1 promotes the emergence of the neoplastic characteristics of BEAS-2B cells

(A) qRT-PCR of COL1A1 transcripts in SE and ME groups. (B) Western blots of COL1A1 in the SE and ME groups. (C) Quantitative analysis results of western blot. (D) BEAS-2B cells were fixed, stained for COL1A1 (green) and DAPI (blue) and imaged with phase and confocal microscopy. (E) Zoom in of stained tissue microarrays. (F) The ratio of possible cells in immunohistochemistry of tissue microarrays. (G) Transwell invasion assays of BEAS-2B cells, R1_05_P50 cells and R25_05_P50 cells transfected with NC or siCOL1A1. (H) Quantitative analysis of transwell invasion assay. I. soft agar colony formation assay in BEAS-2B cells and COL1A1 knockdown cell lines. (J) Quantitative analysis of soft agar colony number. $*p < 0.05$, $****p < 0.0001$.

DISCUSSION

Utilizing the transcriptomics induced by α-particle radiation and protein-protein interaction data, we have proposed a network-based method to try to answer the fundamental question in radiation biology, namely, which effects are induced by high- and low-dose radiation exposure and how this affects the assessment of low-dose cancer risk. First, two exposure-specific networks were constructed by combining gene expression and protein-protein interaction data. Then, a comparison analysis of exposure-specific networks at the global, core network, and module levels was performed to elucidate the molecular mechanisms underlying different irradiation types at the systems level. In addition, we found surprising links between network topology and α-particle exposure phenotypes. Although the two global PPINs of SENet and MENet share similar organizational landscapes, two network parameters, degree and EC, could capture special biological indicators. Several studies suggest that nodes with a high degree are likely to be encoded by essential genes, a phenomenon termed the centrality-lethality rule.[36] In contrast to the degree, EC takes into account the influence of a node's neighbors, which is also a good indicator to identify hub biological pathways and genes.[37] According to its mathematical definition, the higher EC in MENetCore suggests that the network has more robust modules, which are involved in more signal transduction processes. The network results also suggest that multiple low doses of radiation exert a stronger pathogenic effect, especially *via* the ECM-receptor interaction pathway to affect cancer risk.

Research on astronaut health and model organisms has revealed six fundamental biological features resulting from radiation
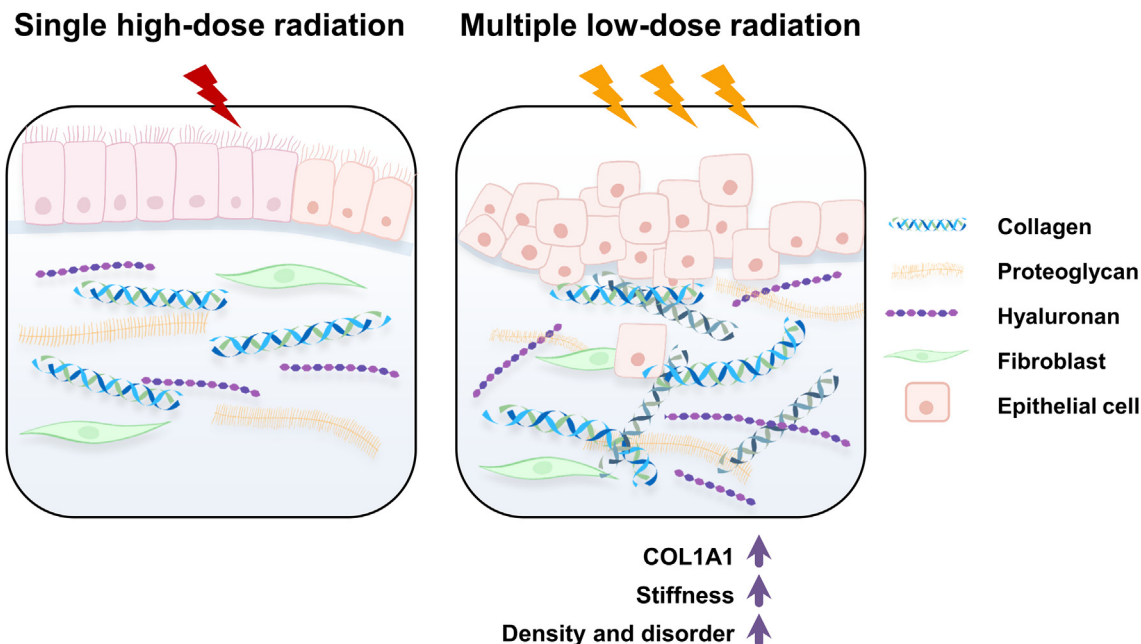
Figure 7. Model of the impact of α-particle radiation on human bronchial epithelial cells
High expression of COL1A1 remodels the ECM organization, increasing ECM density and disorder after multiple low doses of radiation.

exposure, including oxidative stress, DNA damage, mitochondrial dysregulation, epigenetic changes, telomere length alterations, and microbiome shifts.[11] Here, we found that the ECM-receptor pathway was conserved from the whole network to the core network and was the largest module in the ME group. The biophysical characteristics of the ECM strongly regulate cellular responses and are used as indicators of cancer progression and metastasis[38]; hence, it is vital to research the effect of the ECM on tumor development.[39] We thus suggest that the ECM, as a novel cancer hallmark, may be an additional biological feature for multiple low-dose radiation exposures. However, other studies have found that ECM-related pathways are affected by spaceflight[16] and particle radiation.[40] Illa-Bochaca et al.[41] found that particle radiation induces more aggressive tumors and that its carcinogenic effect is mediated by stromal remodeling as well as some signaling pathways in the microenvironment, such as Notch signaling. Yet, how ECM-related pathways contribute to the carcinogenic effect of particle radiation remains unclear. The present work is the first to systematically investigate the transcriptomic effects induced by particle radiation delivered by differential exposure methods, and the results suggest that multiple radiation exposures may affect the expression of collagens, resulting in ECM remodeling in human bronchial epithelial cells.

Collagen is the primary constituent of lung tissue proteins and may be responsible for a plethora of severe lung diseases.[42] Among collagens, type I is the most prominent within the ECM and has a crucial role in sustaining the lung's overall structure[43]; furthermore, COL1A1 serves

as a potential prognostic marker and therapeutic target in lung cancer.[44] In our work, the biological role of COL1A1 in multiple low-dose radiation exposures was further validated by the bioinformatics analyses of lung cancer public databases, a series of biological experiments, and clinical sample research.

Based on our data and observations, we propose possible molecular etiologies of α-particle radiation. As shown in Figure 7, in cells after multiple exposures of low-dose radiation, the expression of COL1A1 was higher, was associated with wider fibers, and caused collagen protein fibers to gradually thicken and change to a linear shape compared with cells with a single exposure of high-dose radiation. The linearized collagen fibers are harder than their coiled counterparts, resulting in an increase in ECM stiffness. This stiffening can significantly enhance ECM density and disorder after irradiation, leading to malignant cell transformation. Due to the pathophysiological and therapeutic potential of both the ECM-related pathway[33] and collagens[45] in cancer, we suggest that COL1A1 may serve as a cancer biomarker in multiple low-dose radiation exposure.

Overall, our work highlights the power of using the differential network method with "omics" data to understand the fundamental biological problem in radiation biology. We found that ECM-receptor pathway dysregulation is a central hub for the effect of low-dose radiation. This new biological feature not only highlights the ECM-receptor pathway together with COL1A1 as a cancer risk in spaceflight, but also suggests a possible approach for pharmaceutical interventions and studies in space biology.

MATERIALS AND METHODS

Cell line

The human bronchial epithelial cell line BEAS-2B was purchased from the American Type Culture Collection (CRL-9609; Rockville, MD, USA) and maintained in DMEM (Gibco, Grand Island, NY, USA) containing 10% fetal bovine serum (FBS) (Gibco Invitrogen, Carlsbad, CA, USA), penicillin (100 U/mL) and streptomycin (100 µg/mL) in a fully humidified incubator with 5% CO_2 at 37°C.

α-particle irradiation

The α-irradiator that we used in this study consisted of a ^{241}Am source, a rotating radiation source holder, a sample holder, and other necessary parts.[46] The ^{241}Am source emitted α-particles at a dose rate of 0.14 Gy/min. The BEAS-2B cells were irradiated either with a single dose of 0.5 Gy one time or were irradiated with 0.02 Gy (9 s of irradiation time) once every 3 days for 25 exposures. Meanwhile, a blank control was set up, which was sub-cultured together with the irradiated group. Thus, the three groups of cells were labeled as the Ctrl (blank control) group, the single exposure (SE) group (0.5 Gy), and the multiple exposures (ME) group (25 single-dose exposures of 0.02 Gy). After all exposures were completed, the cells were continuously sub-cultured to the 10th passage (approximately 3 weeks), 30th passage (approximately 9 weeks), or 50th passage (approximately 15 weeks) and harvested for RNA-seq at various passages. Thus, the SE groups included R1_05_10, R1_05_30, and R1_05_50, and the ME group included R25_05_10, R25_05_30, and R25_05_50.

RNA-seq data profiling and analysis

All cells were harvested in TRIzol reagent (Invitrogen). Total RNAs were reverse-transcribed using the PrimeScript RT Reagent Kit (Takara, Kusatsu, Shiga, Japan). Then, transcriptomics profiling was performed by RNA-seq analysis using an Illumina Novaseq 6000 system by OE Biotech (Shanghai, China). The count level RNA-seq data was used and genes with low expression (count = 0 across more than 80% of samples) were filtered out. rlog normalization and DEG analysis were performed on filtered data using the R package "DESeq2." Genes with an adjusted p value <0.05 and |fold change| >2 were selected as significant DEGs. PCA was performed on the expressional matrix, and all samples were projected onto the two dimensions determined by the first two PCs.

Exposure way-specific PPIN construction

To compare the effects of different exposure methods on the cell ecosystem, we constructed two exposure way-specific PPINs for the SE group and ME group, by integrating the gene co-expression network constructed by WGCNA[47] and the PPIN downloaded from STRING.[48] First, the topological overlap matrix (TOM) was calculated, and a weighted gene co-expression network was constructed using the R package WGCNA based on the gene expression profile of the control group and one of the exposure groups with a soft threshold of 16 for the SE group and eight for the ME group. Next, the network was combined with the human PPIN downloaded from STRING to gain the final exposure way-specific PPIN for the SE group and the ME group, named SENet and MENet, respectively.

Network consistency computation

To measure the consistency of SENet and MENet networks, we calculated the root-mean-square inner product (RMSIP), which measures similarity in the subspace spanned by given eigenvectors, for the TOMs of the two networks.[49] As shown in Equation 1, RMSIP was calculated from the eigenvectors of TOMs.

$$RMSIP = \left(\frac{1}{n} \left(\sum_{i=1}^{n} \sum_{j=1}^{n} \left(V_i . U_j \right)^2 \right) \right)^{1/2} \qquad \text{(Equation 1)}$$

where n is the number of vectors of the matrix, and V_i and U_j are the ith and j^{th} eigenvectors of the TOM$_{SE}$ and TOM$_{ME}$, respectively. We traversed the first 600 eigenvectors of the TOM to calculate the corresponding RMSIP.

Exposure way-specific PPIN core construction and analysis

To reveal the efficient interactions among genes in SENet and MENet, we filtered out the edges with low weight values to keep the high-weighted links and construct the core networks of SENet and MENet, namely, SENetCore and MENetCore. Here, we kept the links with weights larger than 0.4 and 0.45 to construct SENetCore and MENetCore, respectively. The R package "igraph" was employed to calculate the topological parameters degree (K), betweenness (B), closeness (C), and eigenvector centrality (EC) for each node.[50] Their definitions are listed in the supplemental methods.

Robust network module identification

Since the implementation of important biological functions is always in the form of a "module," we identified the robust module in the exposure way-specific PPIN core to indicate the biological function of the network by combining the top-down and bottom-up module discovery methods.[51] Specifically, the weighted Girvan-Newman algorithm and label propagation analysis were used to generate the modules for the network core, and then a hypergeometric test was performed for each pair of modules to find the similarity in the two model results. The overlapping modules with p values <0.05 were considered as robust modules.

Functional enrichment and survival analysis

Functional enrichment analysis and visualization were performed using the R package "clusterProfiler".[52,53] Gene Ontology terms with adjusted p values <0.01 were considered significantly enriched, while the KEGG pathways with p values <0.05 were considered significantly enriched pathways. The survival analysis was conducted by the R packages "survival" and "survminer" based on The Cancer Genome Atlas (TCGA) data.

siRNA mediated COL1A1 gene knockdown

BEAS-2B cells were seeded at 60%–70% confluence prior to transfection. COL1A1-specific siRNA and scrambled siRNA (negative

control) were purchased from Sangon Biotech (Shanghai). Transfections were carried out using Lipofectamine RNAiMAX (Thermo Fisher Scientific) according to the manufacturer's protocol. Cells were harvested 48 h post-transfection for downstream analyses. The target sequences for COL1A1 were as follows: siRNA-1 GGC AAGACAGTGATTGAATAC, siRNA-2 CAAAGGAGACACTGGT GCTAA, siRNA-3 AACCGGAGAACTTACAATAC.

Construction of COL1A1 knockdown cell line using shRNA
A lentiviral vector expressing shRNA targeting COL1A1 was designed and synthesized by Sangon Biotech (Shanghai). The shRNA sequence was selected based on its efficiency in silencing COL1A1 without off-target effects, the TargetSeq of sh-COL1A1-1 is ACAGGGCG ACAGAGGCATAAA, the TargetSeq of sh-COL1A1-2 is CGATGG ATTCCAGTTCGAGTA. The construct contained a GFP marker for selection. Virus production and infection HEK293T cells were transfected with the lentiviral packaging plasmids (pMD2.G and psPAX2) along with the COL1A1-shRNA or scrambled shRNA vector using calcium phosphate transfection. After 48 h, viral supernatants were collected, filtered, and used to infect BEAS-2B cells in the presence of polybrene. Stable transductants were screened by puromycin resistance and verified for GFP expression.

qRT-PCR analysis
A PCR analysis was performed using PowerUp SYBR Green Master Mix (Life Technologies, Grand Island, NY, USA), and amplified PCR products were quantified and normalized with GAPDH. The PCR amplification was carried out using a Life Technologies system (Vii7A) and initiated by 2 min at 95°C before 40 thermal cycles, each consisting of 30 s at 95°C and 40 s at 62°C, with a final extension of 10 min at 72°C. Data were analyzed by Ct value comparison method and normalized by control expression in each sample. The primer sets are listed in Table S3.

Western blotting
Cells were harvested and lysed using RIPA buffer (Beyotime, Shanghai, China). Samples were sonicated and centrifuged at $12,000 \times g$ for 15 min at 4°C. The concentration of total protein was determined using the DC Protein Assay Kit I (Bio-Rad, Richmond, CA, USA). The samples were then denatured at 100°C for 5 min. Total proteins were separated by 12% SDS-PAGE and transferred to Hybond nitrocellulose membranes (Amersham, Piscataway, NJ, USA). The membranes were blocked with 5% nonfat milk powder in Tris-buffered saline (pH 7.5) and hybridized overnight with primary antibodies against COL1A1 and β-actin (Cell Signaling Technology, Danvers, MA, USA). Finally, the membranes were incubated with horseradish peroxidase-conjugated anti-immunoglobulin (Ig)G for 1 h at room temperature and visualized with an ECL kit (Millipore, Billerica, MA, USA). Protein expression levels were normalized to the loading controls based on their intensity analyzed with ImageJ (National Institutes of Health, Bethesda, MD, USA).

Immunofluorescence
BEAS-2B cells were seeded on coverslips in 12-well plates. After irradiation, cells were fixed with 4% formaldehyde in PBS at room temperature for 10 min and then in methanol at −20°C for 20 min, then were permeabilized in 0.1% Triton X-100 in PBS for 10 min and blocked with 5% skim milk for 1 h. Cells were then incubated at room temperature for 2 h with anti-COL1A1 before staining with Alexa Fluor 555 anti-rabbit antibody (Molecular Probes, Eugene, OR, USA) at 37°C for 1 h. Following extensive washing in PBS, the cells were mounted on slides using DAPI mounting medium (Molecular Probes). The stained cells were observed under an Olympus IX71 microscope (Olympus, Tokyo, Japan) and also under a laser scanning confocal microscope (Olympus FV1200, Tokyo, Japan) at Soochow University (Suzhou, China).

Immunohistochemistry of clinical tissue
Non-small cell lung cancer tissue microarrays and patient pathological information were provided by the Department of Pathology of the Second Affiliated Hospital of Soochow University. These lung cancer tissues and matched adjacent normal tissues were reviewed and approved by the Department of Pathology of the Second Affiliated Hospital of Soochow University. All staining was assessed by a quantitative imaging method, and the percentage of positive immunostaining and the staining intensity were recorded. The H-score was calculated using the following formula: H-score = (percentage of cells of weak intensity × 1) + (percentage of cells of moderate intensity × 2) + (percentage of cells of strong intensity × 3).

Cell migration and invasion assays
BEAS-2B cells were plated into 6-well plates and infection was performed when the confluence reached 30%. Briefly, the culture medium was replaced with a mixture of 1 mL of fresh medium and 1 mL of lentivirus suspension. After infection for 24 h, the cells were screened using medium containing 2 μg/mL puromycin (Invitrogen, Carlsbad, CA, USA) for 1 week to establish the cell line with stable COL1A1 knockdown. The lentivirus for COL1A1 knockdown was designed and packed by RiboBio Biotechnology (Guangzhou, China). The stable COL1A1 knockdown was verified by western blot analysis.

The migratory capacity of cells was evaluated using a wound-healing assay. Exposed cells were seeded at a density of 5×10^5 cells/mL/well in a six-well plate. When the cells reached confluence, a scratch was made using a 200-μL pipette tip. Detached cells were washed off and the remaining cells were treated with fresh media without FBS for 48 h. Pictures were taken under a light microscope and the gap width was quantified by using ImageJ software. To evaluate the invasiveness of control and irradiated cells, commercial transwell chambers (24-well plates, 8-μm pore size; BD Biosciences, Franklin Lakes, NY, USA) were used. Briefly, the upper surface of the chambers was coated with 10 μL of matrigel (Corning, Corning, NY, USA). The cells, suspended in serum-free medium, were seeded at a density of 5×10^4 cells/mL/well in the upper chamber, and the lower chamber contained 10% FBS-DMEM. After 48 h of incubation, non-invading

cells were scraped from the upper surface with a cotton swab, and the invading cells at the bottom surface were stained with crystal violet. Stained cells were extracted with 0.5 mL of extraction solution (50:49:1 of ethanol:distilled water:1 M HCl) per well for 10 min with shaking. The optical density of each well was measured at 540 nm.

Lung cancer data collection and analysis

A dataset containing gene expression profiles of 492 patients with lung cancer and 59 normal samples from TCGA was employed for the comparison study. A total of 286 patients with stage I, 122 patients with stage II, and 84 patients with stage III were included in this dataset. The count RNA-seq data were directly used for further analysis.

Statistics

All experiments were independently repeated at least three times, and all data are presented as means ± standard error. Student's t tests were employed for statistical analysis, and a probability (p) value less than 0.05 was considered statistically significant.

DATA AND CODE AVAILABILITY

The α-particle irradiation-induced RNA-seq data have been deposited in NCBI's Gene Expression Omnibus (https://www.ncbi.nlm.nih.gov/geo/) under the accession number GSE235882; lung adenocarcinoma and lung squamous cell carcinoma TNM sample data were downloaded from TCGA. Deposited data and all code are available at GitHub (https://github.com/CSB-SUDA/RDNA).

SUPPLEMENTAL INFORMATION

Supplemental information can be found online at https://doi.org/10.1016/j.omtn.2024.102260.

AUTHOR CONTRIBUTIONS

Conceptualization, W.P., G.Z., G.H.; data curation, W.Y., W.H., Y.S., and W.P.; formal analysis, W.Y., W.H., Y.S., and W.P.; funding acquisition, G.H.; investigation, W.Y., Y.S., and W.P.; methodology, W.Y., X.L.; project administration, G.Z. and G.H.; resources, G.Z. and G.H.; software, X.L. and W.L.; supervision, W.P., G.Z., G.H.; validation, Z.Z., W.L., and Z.C.; visualization, W.Y. and Z.Z.; writing – original draft, W.Y. and G.H.

DECLARATION OF INTERESTS

The authors declare no competing interests.

REFERENCES

1. Garrett-Bakelman, F.E., Darshi, M., Green, S.J., Gur, R.C., Lin, L., Macias, B.R., McKenna, M.J., Meydan, C., Mishra, T., Nasrini, J., et al. (2019). The NASA Twins Study: A multidimensional analysis of a year-long human spaceflight. Science 364, eaau8650.

2. Walls, S., Diop, S., Birse, R., Elmen, L., Gan, Z., Kalvakuri, S., Pineda, S., Reddy, C., Taylor, E., Trinh, B., et al. (2020). Prolonged Exposure to Microgravity Reduces Cardiac Contractility and Initiates Remodeling in Drosophila. Cell Rep. 33, 108445.

3. Yatagai, F., Honma, M., Dohmae, N., and Ishioka, N. (2019). Biological effects of space environmental factors: A possible interaction between space radiation and microgravity. Life Sci. Space Res. 20, 113–123.

4. Moreno-Villanueva, M., Wong, M., Lu, T., Zhang, Y., and Wu, H. (2017). Interplay of space radiation and microgravity in DNA damage and DNA damage response. NPJ microgravity 3, 14.

5. Pariset, E., Bertucci, A., Petay, M., Malkani, S., Lopez Macha, A., Paulino Lima, I.G., Gomez Gonzalez, V., Tin, A.S., Tang, J., Plante, I., et al. (2020). DNA Damage Baseline Predicts Resilience to Space Radiation and Radiotherapy. Cell Rep. 33, 108434.

6. Luxton, J.J., McKenna, M.J., Taylor, L.E., George, K.A., Zwart, S.R., Crucian, B.E., Drel, V.R., Garrett-Bakelman, F.E., Mackay, M.J., Butler, D., et al. (2020). Temporal Telomere and DNA Damage Responses in the Space Radiation Environment. Cell Rep. 33, 108435.

7. Luxton, J.J., McKenna, M.J., Lewis, A., Taylor, L.E., George, K.A., Dixit, S.M., Moniz, M., Benegas, W., Mackay, M.J., Mozsary, C., et al. (2020). Telomere Length Dynamics and DNA Damage Responses Associated with Long-Duration Spaceflight. Cell Rep. 33, 108457.

8. Millar-Wilson, A., Ward, Ó., Duffy, E., and Hardiman, G. (2022). Multiscale modeling in the framework of biological systems and its potential for spaceflight biology studies. iScience 25, 105421.

9. Xu, D., Zhao, X., Li, Y., Ji, Y., Zhang, J., Wang, J., Xie, X., and Zhou, G. (2014). The combined effects of X-ray radiation and hindlimb suspension on bone loss. J. Radiat. Res. 55, 720–725.

10. Azzam, E.I., Jay-Gerin, J.P., and Pain, D. (2012). Ionizing radiation-induced metabolic oxidative stress and prolonged cell injury. Cancer Lett. 327, 48–60.

11. Afshinnekoo, E., Scott, R.T., MacKay, M.J., Pariset, E., Cekanaviciute, E., Barker, R., Gilroy, S., Hassane, D., Smith, S.M., Zwart, S.R., et al. (2020). Fundamental Biological Features of Spaceflight: Advancing the Field to Enable Deep-Space Exploration. Cell 183, 1162–1184.

12. Durante, M., and Cucinotta, F.A. (2008). Heavy ion carcinogenesis and human space exploration. Nat. Rev. Cancer 8, 465–472.

13. Hauptmann, M., Daniels, R.D., Cardis, E., Cullings, H.M., Kendall, G., Laurier, D., Linet, M.S., Little, M.P., Lubin, J.H., Preston, D.L., et al. (2020). Epidemiological Studies of Low-Dose Ionizing Radiation and Cancer: Summary Bias Assessment and Meta-Analysis. J. Natl. Cancer Inst. Monogr. 2020, 188–200.

14. Mullenders, L., Atkinson, M., Paretzke, H., Sabatier, L., and Bouffler, S. (2009). Assessing cancer risks of low-dose radiation. Nat. Rev. Cancer 9, 596–604.

15. Hao, Y., Lu, L., Liu, A., Lin, X., Xiao, L., Kong, X., Li, K., Liang, F., Xiong, J., Qu, L., et al. (2022). Integrating bioinformatic strategies in spatial life science research. Briefings Bioinf. 23, bbac415.

16. da Silveira, W.A., Fazelinia, H., Rosenthal, S.B., Laiakis, E.C., Kim, M.S., Meydan, C., Kidane, Y., Rathi, K.S., Smith, S.M., Stear, B., et al. (2020). Comprehensive Multi-omics Analysis Reveals Mitochondrial Stress as a Central Biological Hub for Spaceflight Impact. Cell 183, 1185–1201.e20.

17. Ray, S., Gebre, S., Fogle, H., Berrios, D.C., Tran, P.B., Galazka, J.M., and Costes, S.V. (2019). GeneLab: Omics database for spaceflight experiments. Bioinformatics 35, 1753–1759.

18. Trinchant, N.M., MacKay, M.J., Chin, C., Afshinnekoo, E., Foox, J., Meydan, C., Butler, D., Mozsary, C., Vernice, N.A., Darby, C., et al. (2020). Clonal Hematopoiesis Before, During, and After Human Spaceflight. Cell Rep. 33, 108740.

19. Malkani, S., Chin, C.R., Cekanaviciute, E., Mortreux, M., Okinula, H., Tarbier, M., Schreurs, A.S., Shirazi-Fard, Y., Tahimic, C.G.T., Rodriguez, D.N., et al. (2020).

Circulating miRNA Spaceflight Signature Reveals Targets for Countermeasure Development. Cell Rep. 33, 108448.

20. Gertz, M.L., Chin, C.R., Tomoiaga, D., MacKay, M., Chang, C., Butler, D., Afshinnekoo, E., Bezdan, D., Schmidt, M.A., Mozsary, C., et al. (2020). Multi-omic, Single-Cell, and Biochemical Profiles of Astronauts Guide Pharmacological Strategies for Returning to Gravity. Cell Rep. 33, 108429.

21. Manian, V., Orozco-Sandoval, J., and Diaz-Martinez, V. (2021). An Integrative Network Science and Artificial Intelligence Drug Repurposing Approach for Muscle Atrophy in Spaceflight Microgravity. Front. Cell Dev. Biol. 9, 732370.

22. Yang, C., Deng, Y., Ren, H., Wang, R., and Li, X. (2020). A multi-channel polymerase chain reaction lab-on-a-chip and its application in spaceflight experiment for the study of gene mutation. Acta Astronaut. 166, 590–598.

23. Lichtblau, Y., Zimmermann, K., Haldemann, B., Lenze, D., Hummel, M., and Leser, U. (2017). Comparative assessment of differential network analysis methods. Briefings Bioinf. 18, 837–850.

24. Leng, J., and Wu, L.Y. (2022). Interaction-based transcriptome analysis via differential network inference. Briefings Bioinf. 23, bbac466.

25. Basha, O., Argov, C.M., Artzy, R., Zoabi, Y., Hekselman, I., Alfandari, L., Chalifa-Caspi, V., and Yeger-Lotem, E. (2020). Differential network analysis of multiple human tissue interactomes highlights tissue-selective processes and genetic disorder genes. Bioinformatics 36, 2821–2828.

26. Savino, A., Provero, P., and Poli, V. (2020). Differential Co-Expression Analyses Allow the Identification of Critical Signalling Pathways Altered during Tumour Transformation and Progression. Int. J. Mol. Sci. 21, 9461.

27. Liu, X., Yang, B., Huang, X., Yan, W., Zhang, Y., and Hu, G. (2023). Identifying Lymph Node Metastasis-Related Factors in Breast Cancer Using Differential Modular and Mutational Structural Analysis. Interdiscip. Sci. 15, 525–541.

28. Gulfidan, G., Turanli, B., Beklen, H., Sinha, R., and Arga, K.Y. (2020). Pan-cancer mapping of differential protein-protein interactions. Sci. Rep. 10, 3272.

29. Huttlin, E.L., Bruckner, R.J., Paulo, J.A., Cannon, J.R., Ting, L., Baltier, K., Colby, G., Gebreab, F., Gygi, M.P., Parzen, H., et al. (2017). Architecture of the human interactome defines protein communities and disease networks. Nature 545, 505–509.

30. Zhou, Z., Lu, Y., Gu, Z., Sun, Q., Fang, W., Yan, W., Ku, X., Liang, Z., and Hu, G. (2023). HNRNPA2B1 as a potential therapeutic target for thymic epithelial tumor recurrence: An integrative network analysis. Comput. Biol. Med. 155, 106665.

31. Ruiz, C., Zitnik, M., and Leskovec, J. (2021). Identification of disease treatment mechanisms through the multiscale interactome. Nat. Commun. 12, 1796.

32. Dang, X., Lin, H., Li, Y., Guo, X., Yuan, Y., Zhang, R., Li, X., Chai, D., and Zuo, Y. (2020). MicroRNA profiling in BEAS-2B cells exposed to alpha radiation reveals potential biomarkers for malignant cellular transformation. Toxicol. Res. 9, 834–844.

33. Huang, J., Zhang, L., Wan, D., Zhou, L., Zheng, S., Lin, S., and Qiao, Y. (2021). Extracellular matrix and its therapeutic potential for cancer treatment. Signal Transduct. Targeted Ther. 6, 153.

34. Koren, E., and Fuchs, Y. (2021). Modes of Regulated Cell Death in Cancer. Cancer Discov. 11, 245–265.

35. Missiuro, P.V., Liu, K., Zou, L., Ross, B.C., Zhao, G., Liu, J.S., and Ge, H. (2009). Information Flow Analysis of Interactome Networks. PLoS Comput. Biol. 5, e1000350.

36. Ahmed, H., Howton, T.C., Sun, Y., Weinberger, N., Belkhadir, Y., and Mukhtar, M.S. (2018). Network biology discovers pathogen contact points in host protein-protein interactomes. Nat. Commun. 9, 2312.

37. Negre, C.F.A., Morzan, U.N., Hendrickson, H.P., Pal, R., Lisi, G.P., Loria, J.P., Rivalta, I., Ho, J., and Batista, V.S. (2018). Eigenvector centrality for characterization of protein allosteric pathways. P Natl Acad Sci USA 115, E12201–E12208.

38. Winkler, J., Abisoye-Ogunniyan, A., Metcalf, K.J., and Werb, Z. (2020). Concepts of extracellular matrix remodelling in tumour progression and metastasis. Nat. Commun. 11, 5120.

39. Pickup, M.W., Mouw, J.K., and Weaver, V.M. (2014). The extracellular matrix modulates the hallmarks of cancer. EMBO Rep. 15, 1243–1253.

40. Chang, P.Y., Bjornstad, K.A., Rosen, C.J., Lin, S., and Blakely, E.A. (2007). Particle radiation alters expression of matrix metalloproteases resulting in ECM remodeling in human lens cells. Radiat. Environ. Biophys. 46, 187–194.

41. Illa-Bochaca, I., Ouyang, H., Tang, J., Sebastiano, C., Mao, J.H., Costes, S.V., Demaria, S., and Barcellos-Hoff, M.H. (2014). Densely ionizing radiation acts via the microenvironment to promote aggressive Trp53-null mammary carcinomas. Cancer Res. 74, 7137–7148.

42. Yuan, Z., Li, Y., Zhang, S., Wang, X., Dou, H., Yu, X., Zhang, Z., Yang, S., and Xiao, M. (2023). Extracellular matrix remodeling in tumor progression and immune escape: from mechanisms to treatments. Mol. Cancer 22, 48.

43. Hou, L., Lin, T., Wang, Y., Liu, B., and Wang, M. (2021). Collagen type 1 alpha 1 chain is a novel predictive biomarker of poor progression-free survival and chemoresistance in metastatic lung cancer. J. Cancer 12, 5723–5731.

44. Pan, B., Huang, C., Xia, Y., Zhang, C., Li, B., Wang, L., Fang, S., Liu, L., and Yan, S. (2022). COL1A1 as a Potential Prognostic Marker and Therapeutic Target in Non-small Cell Lung Cancer. Curr. Bioinf. 17, 909–923.

45. Xu, S., Xu, H., Wang, W., Li, S., Li, H., Li, T., Zhang, W., Yu, X., and Liu, L. (2019). The role of collagen in cancer: from bench to bedside. J. Transl. Med. 17, 309.

46. Ji, W., Tian, W., Yin, X., Yang, H., and Wang, J. (2015). The building and validation of a novel α-irradiation equipment used for cultured cell study. J. Radiat. Res. Radiat. Process. 33.

47. Langfelder, P., and Horvath, S. (2008). WGCNA: an R package for weighted correlation network analysis. BMC Bioinf. 9, 559.

48. Szklarczyk, D., Gable, A.L., Lyon, D., Junge, A., Wyder, S., Huerta-Cepas, J., Simonovic, M., Doncheva, N.T., Morris, J.H., Bork, P., et al. (2019). STRING v11: protein-protein association networks with increased coverage, supporting functional discovery in genome-wide experimental datasets. Nucleic Acids Res. 47, D607–D613.

49. Mishra, S.K., and Jernigan, R.L. (2018). Protein dynamic communities from elastic network models align closely to the communities defined by molecular dynamics. PLoS One 13, e0199225.

50. Liu, C., Ma, Y., Zhao, J., Nussinov, R., Zhang, Y.C., Cheng, F., and Zhang, Z.K. (2020). Computational network biology: Data, models, and applications. Phys. Rep. 846, 1–66.

51. Wang, F., Han, S., Yang, J., Yan, W., and Hu, G. (2021). Knowledge-Guided "Community Network" Analysis Reveals the Functional Modules and Candidate Targets in Non-Small-Cell Lung Cancer. Cells 10, 402.

52. Yu, G., Wang, L.G., Han, Y., and He, Q.Y. (2012). clusterProfiler: an R package for comparing biological themes among gene clusters. OMICS A J. Integr. Biol. 16, 284–287.

53. Wu, T., Hu, E., Xu, S., Chen, M., Guo, P., Dai, Z., Feng, T., Zhou, L., Tang, W., Zhan, L., et al. (2021). clusterProfiler 4.0: A universal enrichment tool for interpreting omics data. Innovation 2, 100141.